THE JOURNAL OF BIOLOGICAL CHEMISTRY VOL. 283, NO. 47, pp. 32925–32936, November 21, 2008

The Stability of the Ternary Interferon-Receptor Complex Rather than the Affinity to the Individual Subunits Dictates Differential Biological Activities*[S]

Received for publication, August 5, 2008, and in revised form, September 15, 2008 Published, JBC Papers in Press, September 18, 2008, DOI 10.1074/jbc.M806019200

Eyal Kalie[‡], Diego A. Jaitin[‡], Yulia Podoplelova[§], Jacob Piehler[§], and Gideon Schreiber[‡1]

From the [‡]Department of Biological Chemistry, Weizmann Institute of Science, Rehovot 76100, Israel and [§]Institute of Biochemistry and Cluster of Excellence Macromolecular Complexes, Goethe University, 60438 Frankfurt/Main, Germany

Type I interferons (IFNs) signal for their diverse biological effects by binding a common receptor on target cells, composed of the two transmembrane IFNAR1 and IFNAR2 proteins. We have previously differentially enhanced the antiproliferative activity of IFN by increasing the weak binding affinity of IFN to IFNAR1. In this study, we further explored the affinity interdependencies between the two receptor subunits and the role of IFNAR1 in differential IFN activity. For this purpose, we generated a panel of mutations targeting the IFNAR2 binding site on the background of the IFNα2 YNS mutant, which increases the affinity to IFNAR1 by 60-fold, resulting in IFNAR2-to-IFNAR1 binding affinity ratios ranging from 1000:1 to 1:1000. Both the antiproliferative and antiviral potencies of the interferon mutants clearly correlated to the *in situ* binding IC_{50} values, independently of the relative contributions of the individual receptors, thus relating to the integral lifetime of the complex. However, the antiproliferative potency correlated throughout the entire range of affinities, as well as with prolonged IFNAR1 receptor down-regulation, whereas the antiviral potency reached a maximum at binding affinities equivalent to that of wild-type IFNα2. Our data suggest that (i) the specific activity of interferon is related to the ternary complex binding affinity and not to affinity toward individual receptor components and (ii) although the antiviral pathway is strongly dependent on pSTAT1 activity, the cytostatic effect requires additional mechanisms that may involve IFNAR1 down-regulation. This differential interferon response is ultimately mediated through distinct gene expression profiling.

Type I interferons (IFNs)[2] form a class of cytokines capable of mediating antiviral, growth-inhibitory and immunoregulatory activities (1–3). Comprising about 18 members in humans (4), all IFNs induce their biological activities through binding to the same receptor complex, composed of the two transmembrane proteins IFNAR1 and IFNAR2 (5). The signal is then transduced mainly through the JAK-STAT pathway, in which the tyrosine kinases Tyk2 and Jak1, which are constitutively associated with the IFNAR1 and IFNAR2 subunits, are activated by phosphorylation upon IFN-receptor binding (6, 7). Subsequently, they phosphorylate STAT proteins that dimerize or form ternary complexes with DNA-binding proteins that translocate to the nucleus to promote the expression of IFN-stimulated genes. The IFNAR1 and IFNAR2 receptor subunits are expressed in virtually every nucleated cell (6), yet the way in which IFNs exert specific activities in different physiological contexts is still obscure. Despite common biological activities, differences observed for various IFNs (8–11) seem to indicate that at least not all IFN subtypes are redundant. Different potencies of specific IFNs are known to be determined to a large extent by their affinities toward the IFNAR1 and IFNAR2 subunits, with only IFNβ standing out for its higher affinity toward IFNAR1 (11). Significant differences are observed in the ability of the two subunits to bind IFNs, as in the case of IFNα2, which binds the IFNAR1 and IFNAR2 subunits with micromolar and nanomolar affinities, respectively. Nevertheless, both components are necessary to induce the IFN signal, as demonstrated by the use of neutralizing antibodies against the extracellular part of IFNAR1 (12) and by a cell line lacking IFNAR2 (13), both resulting in complete lack of responsiveness to both IFNα and IFNβ.

We have recently described an optimized IFNα2 mutant (YNS), which binds IFNAR1 with ~60-fold higher affinity compared with the wild type (K_D = 30 nM) while keeping its affinity toward IFNAR2 unaltered (K_D = 1.5 nM) (14). This is feasible because the binding sites on interferon toward both receptors are located on opposite surfaces and are independent of each other (15–18). In WISH cells, the YNS mutant exhibited a 100-fold stronger antiproliferative potency compared with its wild type counterpart, accompanied by only a slight increase in its antiviral potency, suggesting that IFNAR1 might play a unique role in the induction of IFN-promoted antiproliferative signals and account for differential signaling within this cytokine family (11, 19, 20). Here, we test this hypothesis by analyzing a set of IFNα2 mutants, in which the optimized IFNAR1 binding was combined with a reduction in affinity toward IFNAR2 to various degrees. Our results indicate an additive contribution of both IFNAR1 and IFNAR2 binding to antiproliferative potency along the whole range of mutations, whereas antiviral potency

* This work was supported by Israel Science Foundation (founded by the Israel Academy of Sciences and Humanities) Grant 633/06 (to G. S.) and Deutsche Forschungsgemeinschaft Grants PI 405/4 and EXC 115 (to J. P.). The costs of publication of this article were defrayed in part by the payment of page charges. This article must therefore be hereby marked "*advertisement*" in accordance with 18 U.S.C. Section 1734 solely to indicate this fact.

[S] The on-line version of this article (available at http://www.jbc.org) contains supplemental Scheme 1 and Figs. S1–S3.

[1] To whom correspondence should be addressed. Tel.: 972-8-934-3249; Fax: 972-8-934-6095; E-mail: gideon.schreiber@weizmann.ac.il.

[2] The abbreviations used are: IFN, interferon; JAK, Janus kinase; STAT, signal transducers and activators of transcription; WT, wild type.

reaches a maximum already at low combined affinities. The differential biological effects, which relate to qualitatively different gene expression patterns, are distinctly related to receptor down-regulation and pSTAT1, suggesting that the antiproliferative and antiviral effects are driven by different pathways.

EXPERIMENTAL PROCEDURES

Protein Mutagenesis—Site-directed mutagenesis of IFNα2 was carried out by primer extension using bacteriophage T7 DNA polymerase on expression vector pT7T318U containing the IFNα2 gene, which was used as a single-stranded DNA template following subsequent transfection into and recombinant protein production in CJ236 cells (21).

Protein Expression and Purification—IFNα2 and IFNAR2-EC were expressed in *E. coli* Rosetta strain and purified by ion exchange and size exclusion chromatography (22). Protein concentrations were determined both by analytical gel filtration chromatography and from the absorbance at 280 nm with $\epsilon_{280} = 18{,}500\ \mathrm{cm^{-1}\,M^{-1}}$ for IFNα2 and $\epsilon_{280} = 26{,}500\ \mathrm{cm^{-1}\,M^{-1}}$ for IFNAR2-EC. IFNAR1-EC was expressed in Sf9 insect cells and purified as described before (23).

In Vitro Binding Assays—Binding affinities of IFNα2 toward IFNAR1-EC or IFNAR2-EC were measured using the ProteOn XPR36 Protein Interaction Array system (Bio-Rad), based on surface plasmon resonance technology. Phosphate-buffered saline was used as running buffer at a flow rate of 30 μl/min. For immobilization of the IFNAR1 receptor subunit, a NeutrAvidin-covered sensor chip (NLC; Bio-Rad) was bound with 150 nM biotin-conjugated tris-nitrilotriacetic acid (24). The IFNAR1-EC subunit was then injected to separate channels in duplicates, at 100 and 200 nM, respectively, to bind the tris-nitrilotriacetic acid on the chip surface via their His tags. The IFNAR2 receptor was immobilized as detailed in Ref. 14. The tested interferons were then injected perpendicular to ligands at six different concentrations within a range of 16.5–4,000 nM for IFNAR1 binding and 6.25–200 nM for IFNAR2 binding. Data were analyzed using BIAeval 4.1 software, using the standard Langmuir models for fitting kinetic data. Dissociation constants K_D were determined from the rate constants according to Equation 1,

$$K_D = \frac{k_d}{k_a} \qquad \text{(Eq. 1)}$$

or from the equilibrium response at six different analyte concentrations, fitted to the mass-action equation (22).

Binding Assays on Artificial Membranes—Binding of IFNα2 to IFNAR1-EC and IFNAR2-EC tethered onto artificial membranes was monitored in real time by simultaneous total internal reflection fluorescence spectroscopy and reflectance interference detection in a flow system as in principle described previously (25, 26). Ternary complex formation was probed via the ligand-induced conformational change of IFNAR1 (27). For this purpose, IFNAR1-H10 N349C was cysteine-specifically labeled with ATTO 655 (^{AT655}IFNAR1-H10), which is quenched by the proximal Trp^{347}. Upon ligand binding, the accessibility of Trp^{347} is substantially reduced, leading to dequenching of the dye (27). ATTO 655 was excited by a helium-neon laser (excitation power ~150 microwatts), and the fluorescence was detected through a bandpass filter. Continuous membranes were obtained by fusing lipid vesicles (steroyl-oleyl phosphatidylcholine), which were doped with ~5% lipids carrying tris-nitrilotriacetic acid head groups for tethering the receptor subunits (28) onto clean silica transducer slides. For comparing different combined IFNα2 mutants, IFNAR2-H10 (~3.5 fmol/mm^2) and ^{AT655}IFNAR1-H10 (~2.5 fmol/mm^2) were sequentially tethered onto the membrane. Subsequently, the ligand was injected (100–500 nM), and its dissociation was monitored for 400 s, followed by an injection of imidazole (500 nM) for removing all proteins from the surface prior to the next experiment. The curves were drift-corrected by blank run subtraction, and the dissociation curves were fitted by a two-step dissociation model considering the two equilibria of the binary complexes IFNα2-IFNAR1 and IFNα2-IFNAR2 with the ternary IFNα2-IFNAR1-IFNAR2 complex (26). The differential equations describing the two-step dissociation were fitted using Berkeley Madonna 8.0.1. The parameters for the interaction with IFNAR1 were kept constant for all IFNα2 mutants, and only the two-dimensional dissociation constant for the interaction with IFNAR2 on the membrane was varied. As a control, the binary complex between ^{AT655}IFNAR1-H10 and the IFNα2 mutants was measured, and the dissociation curves were fitted by a monoexponential decay using BIAeval 3.1 software.

In Situ Binding Assays—Wild-type IFNα2 was labeled with ^{125}I using the chloramine T iodination method (29). After iodination, the radiolabeled interferon was cleaned using a homemade Sephadex column. For the competition assay, WISH cells were grown on 24-well plates, washed once with phosphate-buffered saline plus 0.1% sodium azide, and then incubated for 10 min with the same solution. Next, cells were incubated for 1 h at room temperature (20 °C) with the labeled wild type IFNα2 (200,000 cpm/well) in the presence of an unlabeled IFNα2 of interest at 10 different concentrations: wild type IFNα2 and the YNS/153, YNS/148A mutants starting from 50 nM, YNS/30A and YNS/33A starting from 1 μM, and the 30A, 33A, NLYY mutants starting from 6 μM. All tested interferons were diluted in 6-fold steps in culture medium plus 0.1% sodium azide. Cells were then washed twice in phosphate-buffered saline to eliminate unbound interferons, trypsinated, and transferred into test tubes for measuring of bound, ^{125}I-labeled IFNα2 wild type, using a γ-counter (Packard). The experiment was repeated three times, each time in duplicate. IC_{50} values were calculated using Kaleidagraph Synergy Software.

Antiviral and Antiproliferative Assays—The antiproliferative assay (16) was performed on WISH cells by adding the tested IFNα2 (wild type or mutants) at serial dilutions to the growth medium in flat bottomed microtiter plates and monitoring cell density after 72 h by staining with crystal violet. The 50% activity concentrations (EC_{50}) as well as the sensitivity of cells to increasing amounts of interferon were deduced from an IFN dose-response curve (Kaleidagraph, Synergy Software) using Equation 2,

$$Y = A_0 + A/(1 + C/EC_{50})^s \qquad \text{(Eq. 2)}$$

where y represents the absorbance and reflects the relative

number of cells, A_0 is the offset, A is the amplitude, c is the IFN concentration, and s is the slope (16). Antiviral activity was assayed as the inhibition of the cytopathic effect of vesicular stomatitis virus on human WISH cells, as described previously (16, 30). In general, IFN was added at serial dilutions to cells grown on flat bottomed 96-well plates. Four hours later, vesicular stomatitis virus was added to all wells, and after 17 h of incubation, cell density was measured by crystal violet staining. EC_{50} was calculated as described for the antiproliferative experiment. Both the antiviral and antiproliferative assays were repeated at least three times for each protein. The experimental error (σ) for both assays was 35%. Therefore, a confidence level of 2× S.E. would suggest that differences smaller than 2-fold between interferons are within the experimental error.

pSTAT1 and pSTAT3 Phosphorylation Assays—WISH cells were lysed at 4 °C with radioimmune precipitation buffer (150 mM NaCl, 10 mM Tris, pH 7.2, 0.1% SDS, 1% Triton X-100, 1% deoxycholate, 5 mM EDTA). Total protein concentrations were determined using a Bradford assay (Bio-Rad), and equal amounts were separated by SDS-PAGE. Levels of phosphorylated STAT1 and STAT3 were determined by Western blot analysis using polyclonal Tyr(P)^{701}-STAT1- and Tyr(P)^{705}-STAT3-specific antibodies (Santa Cruz Biotechnology, Inc., Santa Cruz, CA). Equal amounts of STAT1 and STAT3 protein were verified by reblotting with a polyclonal anti-STAT1 and -STAT3 antibody (Santa Cruz Biotechnology). Quantitative analyses of the Western blots were done using *ImageJ* software (National Institutes of Health).

Flow Cytometry Analysis of Cell Surface Receptors—Relative levels of IFN receptor subunits were assessed by indirect fluorescence immunostaining and fluorescence-activated cell sorting analysis, as described elsewhere (31, 32). Surface IFNAR levels upon IFN treatment were quantified as relative to untreated cells (100%), using the median value of their signal histograms and taking the isotypic control levels as background.

Gene Expression Profiling—Total RNA was converted to cRNA, labeled, and hybridized on Agilent whole human genome 4X44K (G4112F) microarrays according to the manufacturer's protocol (Agilent). The slides were scanned in an Agilent DNA microarray scanner G2505B. Images were analyzed, and data were extracted using Agilent Feature Extraction software version 9.5.1.1, with linear and Lowess normalization performed for each array. A loop design with two biological replicates was designed to compare the four samples. The statistical analysis was performed using the Limma (Linear Models for Microarray Data) package from the Bioconductor project (available on the World Wide Web). The processed signal resulting from the Agilent Feature Extraction software was read into Limma using the "read.maimages" function. Aquantile normalization between arrays was applied. Standard quality control was performed using the plot functions of Limma (33). Differential expression was assessed using linear models for designed microarray experiments. The -fold changes and S.E. were estimated by fitting a linear model for each gene and applying empirical Bayes smoothing to the S.E. values (34). FDR (false discovery rate) was used to correct for multiple comparisons (35).

RESULTS

Design and Affinity Measurement of Combined IFNAR1/2 Binding Mutations—In all type I interferons, the binding affinity to the IFNAR2 receptor is much higher (up to 1000-fold) compared with the binding affinity to IFNAR1. This raises the possibility that the two receptors have differential roles in signaling, which is the tested hypothesis of the present study. We have recently constructed an optimized IFNα2 mutant designated YNS, which binds IFNAR1 with ~60-fold higher affinity compared with wild type (K_D = 30 nM) while keeping its affinity toward IFNAR2 unchanged (K_D = 1.5 nM) (14). To examine the role of IFN binding to each receptor and correlate the differential affinities with differential biological outputs, we have constructed a series of Ala mutations on the IFNAR2 binding interface of IFNα2 on the background of the YNS mutant, including Ser^{153}, Met^{148}, Leu^{30}, and Arg^{33} (Fig. 1*A*). These mutations were previously found to reduce the binding of IFNα2 WT toward IFNAR2 by 6-, 60-, 700-, and 11,000-fold, respectively (36). Table 1 shows the binding affinities of these mutants as determined by SPR measurements, both on the YNS and WT background, toward IFNAR1 and IFNAR2. In accordance with the notion of independent IFNAR1/2 binding sites on IFN, the alanine mutations located on the IFNAR2 binding site of IFNα2 reduced the affinity toward IFNAR2 to the same extent both in the WT and YNS backgrounds. Accordingly, the affinity toward IFNAR1 of all YNS-containing mutant proteins increased by 50–60-fold, regardless of the reduction in IFNAR2 binding. Overall, these mutants provide proteins with IFNAR2/IFNAR1 binding affinity ratios from 1000:1 down to 1:1000 toward the two receptors, with the YNS/153A mutant having equal binding affinities to both receptors.

Ternary Complex Stability as Measured on Artificial Membranes—In order to explore the consequences of the changes in ligand binding affinities toward IFNAR1 and IFNAR2, we probed ternary complex formation on artificial membranes by simultaneous total internal reflection fluorescence spectroscopy-reflectance interference detection. IFNAR1-EC and IFNAR2-EC were tethered to the membrane via their C-terminal His_{10} tags, which were selectively captured by tris-nitrilotriacetic acid moieties embedded into the membrane, enabling lateral diffusion and ligand-induced ternary complex formation (23, 26, 28). IFNAR1-EC N349C cysteine-specifically labeled with ATTO 655 (^{AT655}IFNAR1-EC) was used for probing binding. The ligand-induced conformational change of IFNAR1-EC strongly reduces the accessibility of Trp^{347}, leading to dequenching of the dye (27). A typical assay is shown in Fig. 1*B*; after sequential tethering of IFNAR2-EC and IFNAR1-EC, the ligand is injected and detected by the increase in fluorescence of ^{AT655}IFNAR1-EC. Whereas on the reflectance interference channel, all ligand binding to the receptor subunits on the membrane is detected, the fluorescence channel selectively detects binding to IFNAR1.

The dissociation curves for different IFNα2 mutants from the ternary complex are compared in Fig. 1*C*. With decreasing affinity toward IFNAR2, faster dissociation from IFNAR1 in the presence of IFNAR2 is observed. On the contrary, in the absence of IFNAR2 on the surface, very similar dissociation

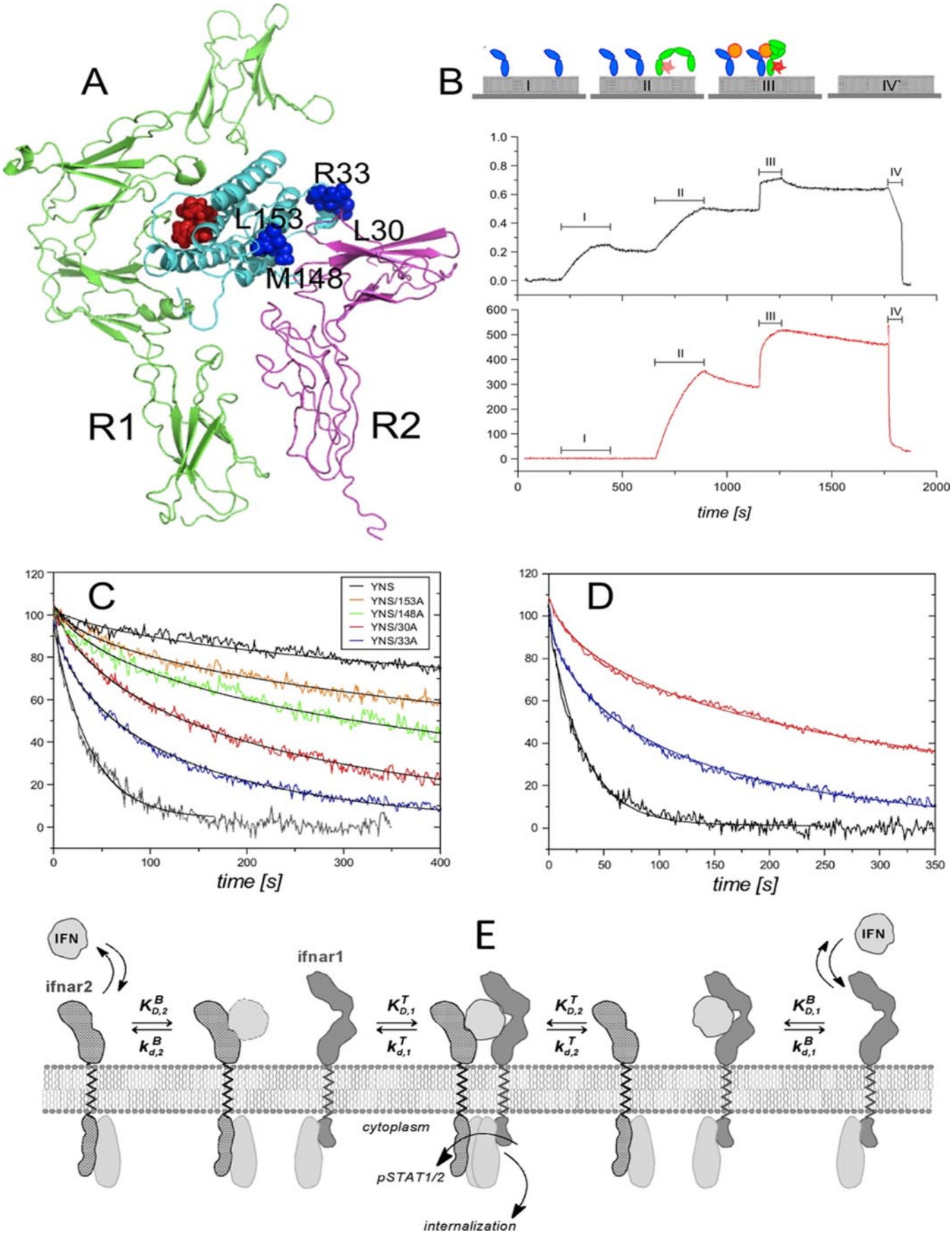

TABLE 1

***In vitro* binding affinities of interferon wild type and mutants towards IFNAR1 and IFNAR2 receptor subunits**

Binding was measured using ProteOn XPR36. K_D values were determined from k_d/k_a over six different concentrations of the analyte. Ratios are relative to wild type IFNα2 (given in the first row). The affinity for IFNα2 was determined using the mass-action equation over six different concentrations of the analyte. The S.E. value for k_a, k_d, and K_D values are 12, 25, and 35%, respectively. ND, below the detection limit.

	IFNAR1		IFNAR2		R2/R1 affinity ratio
	K_D	Ratio (mutant/WT)	K_D	Ratio (mutant/WT)	
	μM		μM		
WT	1.6	1	0.002	1	790
YNS	0.03	53	0.0014	1.4	21
YNS/153A	0.023	70	0.019	0.11	1.2
YNS/148A	0.037	43	0.087	0.023	0.43
YNS/30A	0.03	53	1.8	0.0011	0.018
YNS/33A	0.04	40	29	0.00007	0.0017
30A	3.5	0.5	1.7	0.0012	2
33A	2.8	0.6	29	0.00007	0.1
NLYY		ND	0.003	0.7	

TABLE 2

Binding affinities of IFNs in the ternary complex

IC_{50} values were determined by binding competition assays in WISH cells with ^{125}I-labeled IFNα2 wild type mixed with cold IFN mutants or wild type. Ratios are relative to wild type IFNα2 (given in the first row). The combined affinity (R1 × R2) ratio was calculated by multiplying the relative (to wild type) individual affinity values for IFNAR1 and IFNAR2 taken from Table 1 one by the other. The S.E. is 35%. $t_{1/2}$ values were determined from the dissociaton curves of the ternary complex presented in Fig. 1.

	IC_{50}	Ratio (mutant/WT)	Combined affinity (R1 × R2) ratio	$t_{1/2}$ (ternary complex)	Ratio ($t_{1/2}$)
	nM			s	
WT	0.036	1	1	400	1
YNS	0.0021	18	75	1600	4.1
YNS/153A	0.017	2.1	7.7	600	1.5
YNS/148A	0.16	0.22	1	310	0.79
YNS/30A	0.28	0.13	0.064	140	0.35
YNS/33A	2.7	0.013	0.0028	64	0.16
30A	100	0.00036	0.0012	ND	
33A	1300	0.00003	0.00007	ND	
NLYY	4	0.009	ND	50	0.13

from IFNAR1-EC was confirmed for all IFNα2-YNS mutants (Fig. S1*A*). Substantial stabilization of ligand binding by the presence of IFNAR2 was observed even for IFNα2-YNS/33A (*blue versus gray* in Fig. 1*C*). Although the quenching of ^{AT655}IFNAR1-EC is not directly related to the half-life of the ternary complex (since it is a measure of IFN-IFNAR1 binding), it is qualitatively related. Thus, the half-life extracted from the dissociation curves of the different mutants (Table 2) provides a measure of the stability of the ternary complex. The important role of receptor surface concentration is demonstrated in Fig. 1*D* for IFNα2-YNS/33A; a 3-fold increase in the half-life of the ternary complex is observed upon a 4-fold increase of the receptor surface concentration. Comparison of the dissociation kinetics of IFNα2 WT from the ternary complex measured at a similar receptor surface concentration yields a curve between the curves obtained for IFNα2-YNS/153A and IFNα2-YNS/148A (Fig. S1*B*). A schematic representation of the dynamic stabilization of the ternary complex is presented in Fig. 1*E*.

In Situ Measurements of Ternary Complex Stability on the Cell Surface—Formation of a ternary IFN-IFNAR1/2 complex on the cell surface is necessary to relay an IFN signal into the cell. SPR was used to measure *in vitro* the binding affinities of the different mutants toward each receptor individually, and the measurements on artificial membranes provide us with *in vitro* data on the ternary complex stability. The relevance of the *in vitro* data was then evaluated with *in situ* measurements of the various interferon mutants toward the IFNAR receptors. IC_{50} values were determined using a binding competition assay on the cells with ^{125}I-labeled IFNα2 wild type mixed with cold IFN (either wild type or mutants), measuring residual ^{125}I-labeled IFNα2 binding. The IC_{50} of binding of the four combined mutants as well as L30A, R33A, and NLYY (Ala mutations in residues 65, 80, 85, and 89 resulting in almost no binding to IFNAR1) resulted in micromolar to picomolar values (Table 2 and Fig. S2). Relating the *in situ* EC_{50} values to the combined affinities of IFNs to both receptors (R1 × R2; Table 2 and Fig. 2*A*) as well as to the two receptors bound on artificial membranes (Fig. 1 and Table 2) showed a positive relation between the data. The logic of calculating a combined affinity (R1 × R2) from the individual binding constants is that this represents the simple case where each receptor contributes additively toward the total binding affinity of both receptors to interferon, as seems to be the case on the cell surface. Moreover, the IC_{50} of the wild-type interferon is similar to that measured for the 148/YNS mutant, in agreement with the data presented in Tables 1 and 2 for the combined binding affinities or for binding to both receptors anchored on artificial membranes. This suggests a simple binding model of interferon to both receptors, in which the combined affinity is a function of the additive value of the individual contributions. This concept is further supported by the IC_{50} value for the NLYY mutant (4 nM), which is close to the *in vitro* binding constant determined for IFNAR2 alone using SPR. The half-life of the NLYY mutant as measured in Fig. 1 on artificial membranes was 50 s (Table 2), which is very similar to the value measured for wild-type interferon to IFNAR2 alone, in line with the very weak binding of this mutant to IFNAR1. The weakest IFNAR2 binding mutant tested was R33A, reduc-

FIGURE 1. **Ternary complex formation on artificial membranes.** *A*, ternary structure of the IFN-IFNAR1-IFNAR2 complex (18). Marked in *blue* are mutations facing IFNAR2, and marked in *red* are mutations facing IFNAR1 (YNS). *B*, typical binding assay as detected on the reflectance interference channel (*black*) and the total internal reflection fluorescence spectroscopy channel (*red*). *I*, tethering of IFNAR2-H10; *II*, tethering of ^{AT655}IFNAR1-H10; *III*, binding IFNα2 YNS; *IV*, removal of the proteins by imidazole. *C*, ternary complex dissociation of YNS-IFNα2 bearing mutations at the IFNAR2 binding site in comparison with the dissociation from IFNAR1-H10 alone. All experiments were carried out with ~2.5 fmol/mm^2 ^{AT655}IFNAR1-H10 and ~3.5fmol/mm^2 IFNAR2-H10. *Black lines* correspond to the best fit by a two-step dissociation model. For comparison, dissociation of YNS/33A from ^{AT655}IFNAR1-H10 alone measured under the same conditions is shown in *gray*. *D*, dissociation of IFNα2 YNS/33A at two different receptor surface concentrations of ^{AT655}IFNAR1-H10 and IFNAR2-H10: ~12.5 fmol/mm^2 and ~20 fmol (*red*) and ~2.5 fmol/mm^2 and ~3.5 fmol (*blue*). For comparison, dissociation of IFNα2 YNS/33A from IFNAR1-H10 alone is shown (*black*). *E*, schematic drawing of the IFN-induced assembly of the ternary complex, leading to a dynamic equilibrium between the binary IFN-IFNAR1 and IFN-IFNAR2 and the ternary IFN-IFNAR1-IFNAR2 complexes. The dynamics of the exchange of subunits is determined by the two-dimensional rate constants $k^T_{d,1}$ and $k^T_{d,2}$ (25). The total binding affinity is determined by binary complex equilibrium constants $K^B_{D,1}$ and $K^B_{D,2}$ as well as the equilibrium between binary and ternary complex, which is determined by $K^T_{D,1}$, $K^T_{D,1}$ and the receptor surface concentrations. Altering the binding affinities toward the receptor subunits will affect not only the total binding affinity toward the ligand but also the equilibria between ternary and binary complexes and the dynamics of the exchange.

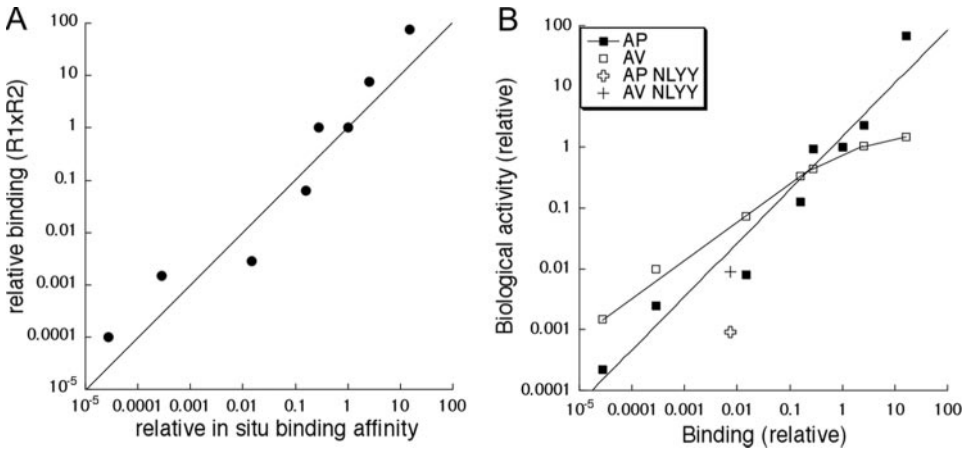

FIGURE 2. **The effect of interferon binding on its activity.** *A*, theoretical *versus* measured affinities of different interferon mutants toward the receptor complex. *X axis*, binding affinities as measured *in situ* in WISH cells; *y axis*, calculated affinities based on the contribution of each receptor subunit alone (R1 × R2), as measured *in vitro* using SPR. *B*, relative biological potency *versus* relative *in situ* affinity of IFNα2 mutants. *X axis*, *in situ* binding affinity relative to wild type IFNα2. *Y axis*, antiproliferative (*AP*) (■) and antiviral (*AV*) (□) potency of combined IFNα2 mutants relative to wild type. *Crosses* represent an IFN mutation with almost no IFNAR1 binding but normal IFNAR2 binding.

TABLE 3
Biological activities and STAT1 phosphorylation
Ratios are relative to wild type interferon (given in the first row).

	Antiproliferative activity		Antiviral activity		pSTAT1	
	EC_{50}	Ratio	EC_{50}	Ratio	EC_{50}	Ratio
	nM		pM		pM	
WT	4.2	1	0.31	1	80	1.0
YNS	0.061	68	0.21	1.5	43	1.9
YNS/153A	1.82	2.3	0.29	1.06	126	0.63
YNS/148A	4.4	0.94	0.69	0.45	184	0.43
YNS/30A	32	0.13	0.9	0.34	821	0.1
YNS/33A	510	0.0082	4.2	0.073	1100	0.07
30A[a]		0.0025		0.01	5000	0.016
33A[a]		0.00022		0.0015	ND	ND
NLYY[b]		0.0009		0.01	1150	0.07

[a] Ratios taken from Ref. 36 using WISH cells for antiviral and Daudi for antiproliferative activity.
[b] Ratio taken from Ref. 16.

ing binding to IFNAR2 to 29 μM. The *in situ* IC_{50} values of 1.3 μM and 3 nM for this mutant in the absence and presence of the YNS mutations demonstrate the synergistic binding to both receptors. These biological binding data, measured on WISH cells by titration experiments, validate the relevance of the *in vitro* data for further correlation with the exclusive effects of IFNAR1 and IFNAR2 on the biological activity of IFN.

Antiproliferative and Antiviral Activities Are Differently Affected by Mutations on Interferon—The biological activity of the different mutants was tested in WISH cells. In this cell line, the initiation of the antiviral state requires at least 4 h of IFN treatment at pM concentrations, whereas antiproliferative (apoptotic) activity is measured only after 72 h and requires IFN in nanomolar concentrations. In this cell line, the YNS mutant is a much stronger activator of the antiproliferative effect than wild-type IFNα2 (100-fold increase), whereas its EC_{50} value for antiviral activity is hardly changed (Table 3). We were therefore interested in determining whether IFNAR1 has an exclusive effect on the antiproliferative activity. Antiproliferative and antiviral potencies of the interferon mutants in WISH cells were determined from the EC_{50} values as calculated from dose-response curves (Table 3). The antiproliferative activity correlated with the *in situ* binding affinity (Fig. 2*B*), whereas for the antiviral activity, this correlation was observed only for affinities lower than wild type. In addition, different slopes of 0.53 and 0.88 were observed for the antiviral and antiproliferative effects, respectively. Thus, the antiviral activity seems to approach a saturated phase, where it is less sensitive to further changes in the affinity, as opposed to the antiproliferative activity that is highly affected by affinity changes throughout the entire given range. In addition, the NLYY mutant, which has no measurable IFNAR1 binding *in vitro* (16), exhibited a distinctive behavior with activities lower than one would expect from its overall *in situ* affinity. These data are in line with our notion that NLYY binds normally to IFNAR2 (with nanomolar affinity) but binds IFNAR1 very weakly and therefore hardly promotes the formation of the ternary complex, which is critically required for biological activity.

STAT1 Phosphorylation Follows the Same Pattern as Antiviral, but Not Antiproliferative Activity—We next sought to define the relation between the binding affinities of the IFN mutants and phosphorylation of STAT1, a major signaling factor in the JAK-STAT pathway associated with IFN signaling. pSTAT1 levels on tyrosine 701 reach a maximum after the first 1 h of interferon induction, after which pSTAT1 declines back to noninduced levels (14, 32). On the contrary, the total STAT1 (and STAT2 but not STAT3) protein levels rise only after more than 8 h of continuous induction (32). Therefore, WISH cells were treated with the various mutants at different concentrations (2.5–800 pM) for 45 min in order to assess pSTAT1 by Western blot using $Tyr(P)^{701}$-STAT1-specific antibodies (Fig. 3*A*). For all measurements, levels of general protein were similarly assessed using the appropriate antibodies, showing no increase in protein concentrations for all treatments. As seen in Fig. 3*A*, STAT1 phosphorylation levels were similar for YNS, WT, YNS/153A, and YNS/148A and reduced for the other mutants, with no pSTAT1 observed at concentrations up to 800 pM for the R33A mutant. The same pattern of induction was observed also for STAT3 phosphorylation (Fig. 3*A*, *right*). To further quantify the levels of pSTAT1, the Western blots shown in Fig. 3*A* were scanned, quantified, and normalized against total protein levels (Fig. 3*B*). Phosphorylation values were then plotted *versus* the IFN concentration, from which the EC_{50} values were determined using Equation 2 and are shown in Table 3. No large differences in EC_{50} for pSTAT1 or pSTAT3 relative to WT were detected for YNS and YNS 153A (Table 3 and Fig. 3*A*). Comparing the phosphorylation levels of STAT1 and STAT3 with the activity profiles for each mutant (Table 3 and Fig. S3) clearly shows that the antiviral potency

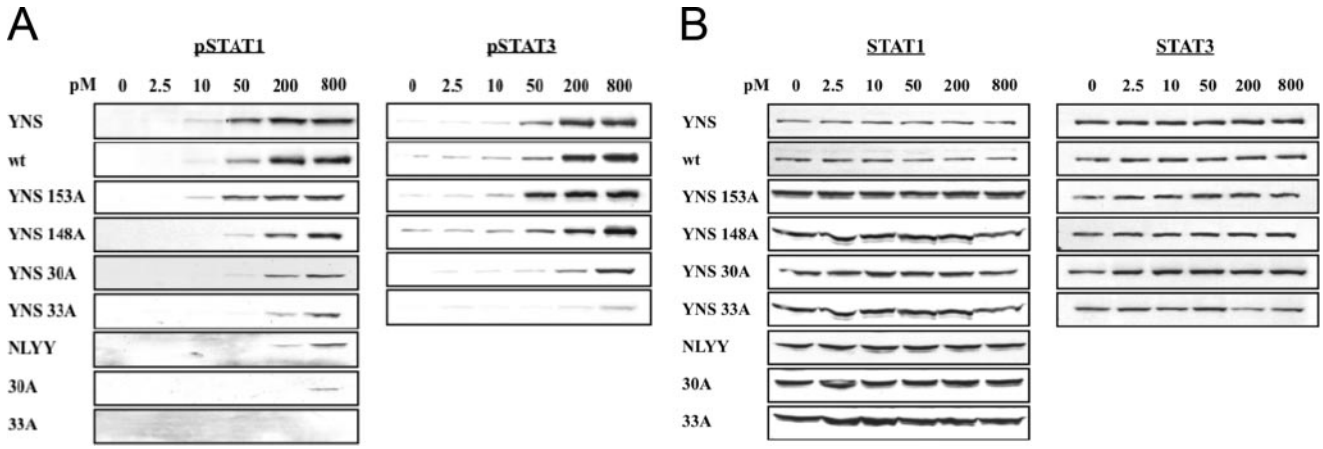

FIGURE 3. **Activation of STAT1 and STAT3 by the combined IFN mutants.** *A*, STAT1 and STAT3 phosphorylation induced by the combined IFNα2 mutants, detected by Western blots using Tyr(P)^{701}-STAT1- and Tyr(P)^{705}-STAT3-specific antibodies. *B*, levels of total STAT1 and STAT3 proteins of the same blots, detected by specific general STAT1 and STAT3 antibodies.

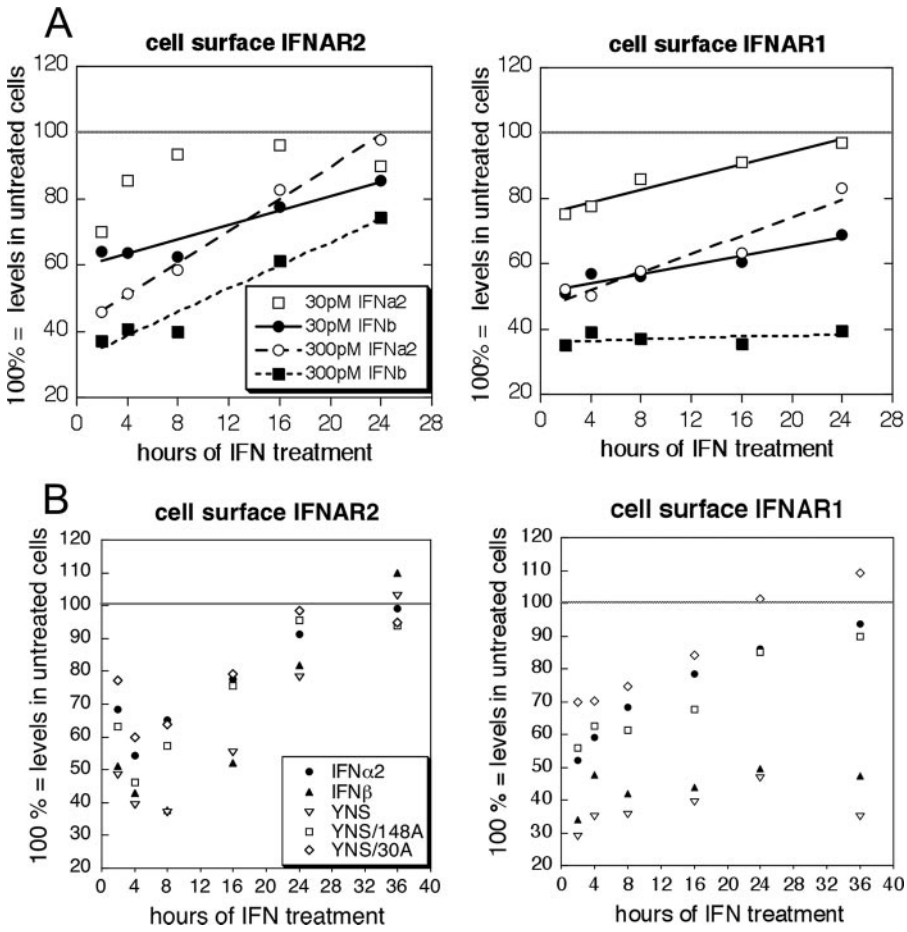

FIGURE 4. **Change in receptor surface levels following interferon treatment.** *A*, levels of surface IFNAR1 and IFNAR2 subunit after different incubation times with either IFNα2 or IFNβ at 30 and 300 pM. *B*, levels of surface IFNAR1 and IFNAR2 subunit following treatment with 100 pM mutant IFNs. All measurements were done using fluorescence-activated cell sorting analysis in WISH cells. The *gray line* at 100% represents the measurement done at the same time points without treatment. The different time points are averages from at least two independent measurements.

of these mutants follows a similar trend as pSTAT1 and pSTAT3, whereas the antiproliferative activity does not. Moreover, both pSTAT1 levels and antiviral potency reach a maximum once the EC_{50} of interferon binding to the surface receptor reaches the level of wild type IFNα2 and do not increase further (Table 3 and Fig. S3). On the contrary, the antiproliferative activity of the different mutants is not related to the pSTAT1 activation pattern.

Differential Down-regulation of the IFNAR Receptor Subunits Is Dictated by the Integral Lifetime of the Receptor-IFN Complex—IFNAR receptor down-regulation is generally accepted as a means of signal attenuation following an IFN stimulus. In a recent report, it was shown that cell surface IFNAR internalization is actually required for a full and fast transduction of the IFN signal (37). Treatment with different IFN subtypes, namely IFNα2 *versus* IFNβ, resulted in a differential down-regulation of the IFNAR subunits (32). Particularly, IFNAR1 was down-regulated after 16 h of treatment with IFNβ but not IFNα2. This finding raised a question regarding the role of internalization in differential IFN signaling. Receptor numbers on the surface of WISH cells were quantified here by fluorescence-activated cell sorting following interferon treatment. We first compared IFNα2 with IFNβ at 30 pM, a concentration below a full antiproliferative effect in WISH cells for both IFNs, and 300 pM, at which only IFNβ can promote a full antiproliferative response (31). During the course of IFN treatment at low concentrations, both IFNAR subunit levels were initially down-regulated, followed by a linear recovery over time, as expected (Fig. 4*A*).

A

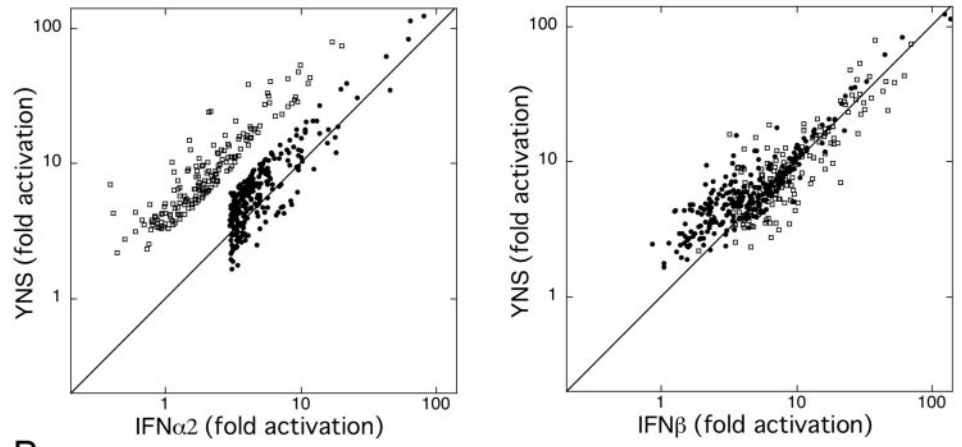

B

Functional gene annotation after 36 hr of treatment and their clustering using David

135 genes that are differentially up-regulated by YNS in respect to IFNα2 (panel A open squares)

Term	Count	P-Value
immune system process	29	3.30E-09
immune response	24	7.90E-08
response to external stimulus	18	1.90E-06
response to stimulus	43	2.40E-06
cytokine	10	2.80E-06
receptor binding	19	3.40E-06
cytokine activity	11	6.00E-06
cell activation	10	3.90E-05
response to wounding	13	4.10E-05
inflammatory response	11	4.40E-05
Cytokine-cytokine receptor interaction	13	6.80E-05
locomotory behavior	9	6.80E-05
taxis	8	7.70E-05
chemotaxis	8	7.70E-05
leukocyte activation	9	1.00E-04
Small chemokine, interleukin-8-like	5	1.20E-04
G-protein-coupled receptor binding	6	1.50E-04

188 genes that are equally up-regulated by YNS together with IFNα2 (panel A solid circles)

Term	Count	P-Value
immune response	40	2.40E-16
response to virus	16	1.20E-14
immune system process	41	6.70E-14
response to biotic stimulus	22	7.30E-13
antiviral defense	10	4.30E-11
response to stimulus	61	3.60E-10
response to other organism	16	3.90E-10
Type I diabetes mellitus	9	8.60E-09
MHC I	8	8.80E-09
antigen processing and presentation of peptide via MHC I	9	1.70E-08
multi-organism process	17	3.20E-08
MHC class I protein complex	9	1.20E-07
MHC class I receptor activity	6	7.80E-07
defense response	20	1.10E-06
Antigen processing and presentation	9	2.80E-06
Immunoglobulin/major histocompatibility complex motif	11	2.90E-06
MHC class I-like antigen recognition	7	1.20E-05

FIGURE 5. **Effect of IFN on gene expression.** We compared the expression profiles of three conditions consisting of WISH cells incubated for 36 h with 0.1 nM IFNα2 WT, YNS, or IFNβ. After normalization, the genes were sorted according to their level of induction by YNS relative to IFNα2. A set of 135 differentially (>3-fold) induced genes (*open squares*) and a set of 188 equally induced genes (*solid circles*) were retrieved. *A*, normalized gene induction by YNS treatment (*y* axis) plotted against normalized gene induction by IFNα2 WT (*x* axis, *left plot*) or IFNβ (*x* axis, *right plot*). For both sets of genes, no significant change in the level of induction is observed between YNS and IFNβ. *B*, the two sets of genes were subjected to gene annotation analysis using the bioinformatics resource DAVID (available on the World Wide Web), which identified enriched biological processes. These were clustered using the cluster algorithm in DAVID and marked by *colors* according to cluster.

However, at 300 pM IFNβ (but not IFNα2), the down-regulation of IFNAR1 was sustained for the entire length of the experiment (24 h), whereas surface expression levels of IFNAR2 returned to normal. To eliminate reduced IFNAR transcript levels as a possible explanation for the observed down-regulation, we analyzed receptor mRNA levels on an Agilent gene chip (see Fig. 5) and found no change in IFNAR1 and a small (1.6-fold) increase in IFNAR2 mRNA levels after 36 h of treatment, independent of the interferon used.

Using the combined mutants, we were able to test whether the sustained IFNAR1 down-regulation was the result of a higher affinity of IFN toward IFNAR1 or a higher affinity toward the ternary complex in general. If high affinity toward IFNAR1 alone is sufficient, these combined mutants will still induce prolonged down-regulation of IFNAR1, similar to YNS or IFNβ. We measured the levels of cell surface IFNAR subunits upon incubation with these IFN mutants at 100 pM, a concentration that is sufficient to induce a maximal antiproliferative response with IFNβ and YNS but not with IFNα2. Again, the early down-regulation of IFNAR2 was followed by linear recovery (Fig. 4*B*). Only IFNβ and the YNS mutant induced a continuous differential IFNAR1 down-regulation at this concentration. Strikingly, the YNS/148A mutant and IFN-α2 WT, which have comparable combined affinities, induced similar IFNAR1 down-regulation patterns. The YNS/30A mutant promoted the weakest IFNAR1 down-regulation, in agreement with its weak combined affinity. These results show that a high affinity toward IFNAR1 is not sufficient to induce its prolonged down-regulation. Rather, differential receptor down-regulation is dictated by the integral lifetime of the ternary receptor-IFN complex. This can result from high binding affinity to the receptors, such as in the case of YNS or IFNβ, or high concentration of weaker binding interferons, such as 3 nM IFNα2, which also induced prolonged IFNAR1 down-regulation as well as antiproliferative activity (data not shown). Importantly, these data exhibit an intriguing correlation between differential receptor down-regulation and the antiproliferative potency.

IFN-induced Gene Regulation—We have previously shown that after 16 h of treatment with interferon, the gene induction profile of the IFNα2 triple mutant HEQ (57A, 58A, 61A) is similar to that of IFNβ and quantitatively, but not qualitatively, different from that observed for IFNα2 (31). Bearing in mind that for a cytostatic effect, a prolonged exposure of target cells to IFN is required, we analyzed here the gene induction profile after 36 h of induction with 100 pM IFNα2, YNS, or IFNβ. This concentration was chosen, since it promotes antiproliferative activity using YNS and IFNβ but not using IFNα2 (yet is far above the concentration required for a full antiviral activity for all three) (Table 3) (14). Contrary to our observations following 16 h of IFN treatment, at 36 h we already observed a qualitative difference in gene activation. Of particular interest are those genes that are differentially up-regulated at 36 h of YNS or IFNβ but not IFNα2 treatment (Fig. 5*A*). By sorting the expression data according to their -fold change upon YNS or IFNα2 induction, we found a set of 135 genes that were differentially up-regulated (at least 3-fold stronger for YNS compared with IFNα2) and 188 genes that were equally up-regulated (by at least 3-fold) in both treatments (Fig. 5*A*).

Next, we used the DAVID bioinformatics resource (available on the World Wide Web) to functionally annotate these two gene sets. Fig. 5*B* shows the ~20 most up-regulated gene functions, clustered into six families (sorted by DAVID). The two gene sets are distinct in their functions. The equally up-regulated genes code for genes involved in direct response to viruses and other pathogens as well as for up-regulation of the major histocompatibility complex I response. Conversely, the YNS differentially up-regulated genes code for inflammation and cytokine and chemokine functions. Both sets have in common the activation of the immune system. Although the difference in gene activation is quantitative, the prolonged YNS *versus* IFNα2 treatments code for a qualitative difference in the way the cellular defense is activated.

DISCUSSION

The differential activation of cells by IFNs through a shared cell surface receptor calls for a molecular explanation. IFNs exert their activity through the binding to two different receptor subunits, and it has been suggested that each subunit possesses specific signaling capabilities. Recent findings have established a key role for ligand binding affinity toward IFNAR1 in differential activation (11, 31, 37, 38). Here, we have aimed to systematically define the relation between ligand binding affinities toward the individual subunits, the formation of the ternary complex, and the activation of signaling pathways and different cellular responses. For this purpose, we engineered a panel of IFNα2-based mutants binding IFNAR1 and IFNAR2 at affinity ratios ranging from 1000:1 to 1:1000. These mutants cause a reduction in IFNAR2 binding to different extents, whereas IFNAR1 binding is significantly enhanced using the IFNα2-YNS triple mutant that binds IFNAR1 60-fold tighter than wild type. We also used the NLYY mutant, where IFNAR1 binding is reduced by ~100-fold. Affinity changes toward the two receptor subunits were verified by SPR using purified receptor subunits, on solid-supported membranes with the two receptors immobilized, and on the cell surface using ^{125}I-labeled interferon. The affinities of these ligands toward both receptors *in vitro* and on the cell surface correlated well with the theoretically estimated affinity from the contribution of each receptor subunit, corroborating independent ligand binding sites on IFNAR1 and IFNAR2. This is in line with the distinct location of the binding sites of the two receptor subunits on interferon (Fig. 1*A*).

Using these mutants, we observed a clear linear correlation between the relative antiproliferative potencies and the relative cell surface receptor binding affinities with a slope of ~1. These findings suggest a simple additivity, rather than cooperativity, in the binding of the two receptors and establish that the total binding affinity, but not the particular affinity toward one of the receptor subunits, dictates the antiproliferative activity of IFNs. A rather simple model for antiproliferative IFN signaling emerges from these results, which is determined by two factors: the rate of complexation events and the stability of the ternary complex once it is formed. The latter is a function of the affinity toward both receptors and the concentration of all components (Fig. 6). Thus, high interferon or receptor concentrations may compensate for low binding affinities, as is indeed observed (11, 31). In contrast, the relationship between the relative antiviral potencies of the different mutants and the binding affinities is more complex. Antiviral activity reaches a level close to maximum (in WISH cells) when the combined affinity to both receptors (R1 × R2) is that of wild-type IFNα2 (14). A similar phenomenon of maximal cellular activity independent of the affinity was previously found for human growth hormone (39). However, we show here that the maximal antiviral activity is related to the overall receptor binding affinity, independent of whether it results from a tighter IFNAR1 or IFNAR2 binding. This is clearly demonstrated by the YNS/153A and YNS/148A mutants; these have a wild-type-like antiviral potency, dictated by their total binding affinity to the cell surface receptor that is close to the wild-type protein, although IFNAR1 binding is strengthened and IFNAR2 binding is weakened in these mutants. Interestingly, the slope of the antiviral-affinity relation is only ~0.6 and not close to the expected slope of 1, as observed for the antiproliferative activity.

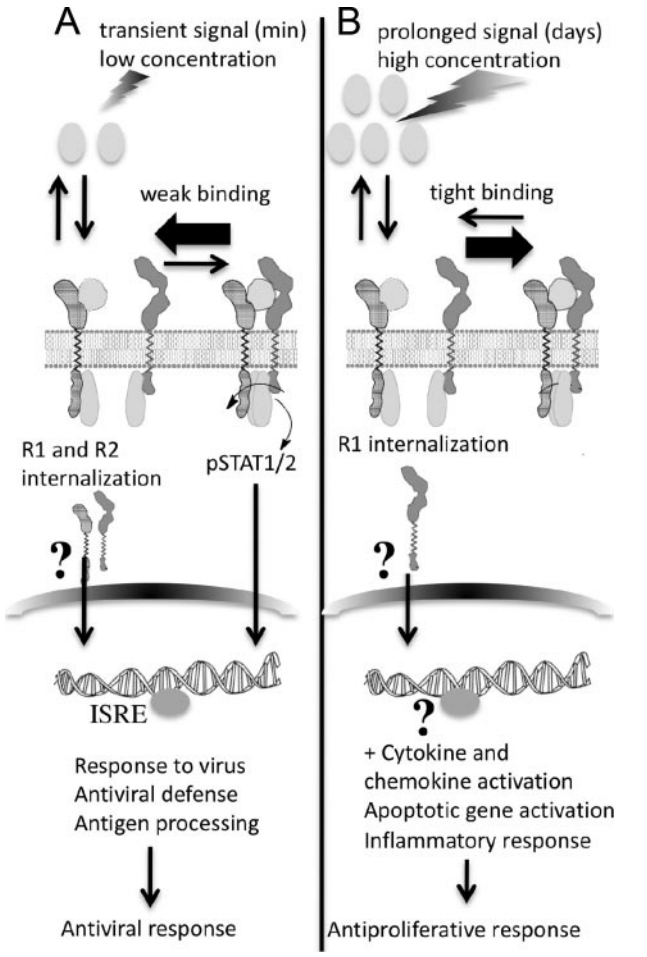

FIGURE 6. **A schematic view on differential activation by interferons.** *A*, the pathway of antiviral response, initiated by a transient signal of low concentration of weaker binding interferons. *B*, the pathway of antiproliferative response in WISH cells, initiated by a prolonged signal of higher concentration of tighter binding interferon.

Since these differences in the affinity-activity correlations for antiviral and antiproliferative responses may define the differential signaling patterns of IFNs, we analyzed the downstream consequences of differential receptor binding affinities. We

found that pSTAT1 or pSTAT3 activation relates to the stability of the ternary complex, with a similar trend as the antiviral but not antiproliferative activity (Fig. S3). These data support the notion that accumulation of pSTAT1 and pSTAT3 is directly related to the initiation of an antiviral state (Fig. 6). In contrast, antiproliferative activity seems to be related not only to the STAT pathway but to an additional STAT-independent pathway, which is activated in a linear activity-affinity relationship.

An interesting characteristic of the antiviral activity lies in its low EC_{50} value, which is 0.3 pM for IFNα2, whereas the EC_{50} of *in situ* receptor binding and pSTAT1 activation is ~50 pM. These results suggest that activation of a minor part of the cell surface receptors and thus the induction of submaximal STAT phosphorylation is sufficient to promote full antiviral protection (~1% receptor occupancy provides 50% protection). In contrast, antiproliferative activity requires ligand concentrations well above the EC_{50} of the cell surface receptor binding. We suggest that these observations can be explained by the kinetics of receptor binding and dissociation. We have previously demonstrated on artificial membranes that the ternary IFN-receptor complex is in dynamic equilibrium with the binary complexes of IFN with IFNAR1 and IFNAR2, as schematically depicted in Fig. 1*E* (25). Differences between the binding affinity of IFNs toward the receptor subunits will change the equilibrium concentrations of binary and ternary complexes as well as the dynamics of the equilibrium. The lifetime of the ternary complex is limited by the shorter lifetime of the interaction with either one of the receptor subunits, leading to a faster exchange of the receptor subunits. It appears that STAT phosphorylation (and thus the induction of an antiviral response) does not require a stable ternary complex; even for YNS/33A, with an estimated lifetime of ~20 ms for the IFN-IFNAR2 interaction, some STAT phosphorylation is observed. Since phosphorylation is a very fast process (millisecond range), longer complex lifetimes are probably not required. It is even possible that rapid exchange of receptor subunits promotes STAT phosphorylation, since mutants with a short lifetime of interaction with IFNAR2 (*e.g.* IFNα2 L30A) show relatively high STAT phosphorylation and antiviral activity compared with their binding affinity to the cell surface receptor.

To further quantify the STAT1 phosphorylation pattern, we simulated the rate of accumulation of pSTAT1 in cells using the Pro-Kineticist II software, a second order global kinetic analysis software (Applied Photophysics Ltd.). We used the model presented in supplemental Scheme 1, which contains in addition to the equilibrium between the different forms of the interferon-receptor complex (as presented in Fig. 1*E*) also a term for activation (by Tyk2) and deactivation (by either SOCS or receptor endocytosis) of the phosphorylated, active ternary complex. The simulations show similar $pSTAT1_{50}$ levels (the IFN concentration giving 50% pSTAT1) for wild-type IFNα2, YNS, YNS/153A, and YNS/148A. Weaker binding mutants, such as YNS/30A, L30A, and NLYY, have lower calculated $pSTAT1_{50}$ values, which correlate well with the experimental data. The predictive nature of the calculations was independent of whether the affinity to IFNAR1, IFNAR2, or both were altered. The simulations suggest that the rate of deactivation of the active (STAT1 binding) ternary complex becomes the rate-limiting factor once the lifetime of the ternary complex exceeds that observed for wild-type IFNα2. Therefore, further stabilization of this complex by mutations, such as YNS (as seen in Fig. 1), has no effect on STAT1 phosphorylation. However, for weaker binding mutants, the lifetime of the active receptor complex is dictating the rate of pSTAT1 accumulation. The different rate-limiting steps along the reaction are also the reason for the slope of less than 1 observed for the relation between binding affinity and pSTAT1 accumulation (and antiviral activity).

Rapid, ligand-induced down-regulation of both IFNAR1 and IFNAR2 (endocytosis) has been previously reported (40–43). This down-regulation was indeed shown to affect IFN signaling, both by signal attenuation (38) and direct involvement in signal propagation (37). Reduction in cell surface concentrations of one or both of the receptor subunits reduces cell sensitivity and alters further signaling (37, 38, 40, 44, 45). Moreover, a clear correlation was suggested between the efficiency of interferon as a cancer drug and surface receptor concentration (38, 46, 47). In a recent study, Marijanovic *et al.* (40) showed that the cell surface IFNAR1 level is indeed a limiting factor for assembly of the functional complex, but an increased concentration of it does not translate into an IFNα/β differential JAK-STAT signaling; nor does it change the dynamics of the engaged receptor. Tyk2 and receptor ubiquitination were identified as the main factors controlling the endocytosis of IFNAR and its routing to degradation *versus* recycling (48–50). However, all of these studies probed only the first few hours after interferon induction and not the long term effects described in this paper. Rapid receptor down-regulation and STAT activation is observed on a time scale of hours. However, antiproliferative activity works on the time scale of days (Fig. 6). We found here that IFNAR1 and IFNAR2 follow a differential down-regulation pattern after continuous treatment for 36 h. Upon treatment with either IFNα2 or IFNβ, membrane, IFNAR2 is rapidly down-regulated but returns to normal concentrations within 36 h of treatment. On the contrary, IFNAR1 down-regulation is more complex. Following 2 h of treatment, IFNAR1 is down-regulated, independent of the interferon used. However, although IFNAR1 cell surface concentrations recover for IFNα2-treated cells with a similar kinetics as observed for IFNAR2, IFNβ- or YNS-treated cells maintain substantially lower concentrations of IFNAR1 (around 40% of basal level) even after 36 h of treatment. In light of the high affinity of IFNβ and YNS toward IFNAR1, we initially suspected that IFNAR1 binding by itself might account for this phenomenon. However, fluorescence-activated cell sorting measurements of the combined mutants (YNS/148A or YNS/30A) revealed that IFNAR1 down-regulation correlates with the overall stability of the ternary complex (which is limited by the weakest interaction) and not necessarily with the stability of IFN-IFNAR1 interaction. We therefore conclude that the long term differential pattern of receptor down-regulation is proportional to both receptor subunit affinities in an additive manner, thus rejecting the possibility of a unique role for IFNAR1 in initiating this pattern. These low expression levels of IFNAR1 on the membrane are likely to reduce responsiveness of the cells to some IFNs, perhaps giving an advantage to strong IFNAR1/2 binders. A similar down-regulation pattern was shown in human dendritic cells by Severa *et al.* (44),

where autocrine release of IFNβ caused a long term reduction of IFNAR1 but not IFNAR2 levels on the cell membrane. These cells were indeed desensitized to IFNα2 treatment, whereas their responsiveness to IFNβ treatments remained normal.

Importantly, the differential IFNAR1 down-regulation pattern closely follows the antiproliferative signal in terms of signal duration, affinity toward the receptor, and interferon concentrations needed for prolonged IFNAR1 down-regulation, whereas pSTAT1 activation follows the antiviral signal. Along with our observation that the antiviral potency of IFNs, but not their antiproliferative potency, is naturally close to saturation levels, these observations support the idea of a pSTAT1-independent pathway(s) required for antiproliferative signaling (Fig. 6). Nuclear localization and transactivation activity was recently reported for IFN-γ and its IFNGR1 receptor subunit (51), and since IFNAR1 contains a nuclear leading sequence (41), it is likewise tempting to speculate that following endocytosis, this receptor subunit acts as an intracellular signaling factor, mediating the expression of key antiproliferative genes. Further investigation into the fate of IFNAR1 once internalized in the cell may provide important insights on the differential signaling of IFNs.

Gene activation patterns after 36 h of constant treatment with IFN confirmed a clear qualitative difference between YNS- and IFNα2-induced gene activation, with YNS inducing a similar pattern as IFNβ. Those genes that are up-regulated by all three IFNs relate to antiviral and major histocompatibility complex I functions, whereas the differentially up-regulated genes (by YNS and IFNβ) relate to inflammation and cytokine and chemokine responses. These results strengthen our notion that differential interferon action is indeed related to the binding affinity toward the ternary complex, the time of activation, and the concentration of the interferon and that these dictate a clear difference in the physiological outcome.

In summary, systematic variation of subunit binding affinity has revealed that the nonlinear correlation of antiviral activity and cell surface receptor binding leads to differential activity patterns of IFN (Fig. 6). We speculate that the stabilization of the ternary complex on the membrane, together with the rate of deactivation of the signaling complex lead to the nonlinearity of pSTAT1 activation, which in turn leads to the nonlinear effect (in respect to binding affinity) of the antiviral response. Moreover, we postulate a pSTAT-independent pathway responsible for antiproliferative activity, which strictly depends on ligand binding affinity and is correlated with IFNAR1 down-regulation. A differential set of genes is activated by this pathway, yet so far we could not identify a common transcription factor driving differential gene production. However, whether binding is tighter to IFNAR1 or IFNAR2 is not a major factor in differential activation.

Acknowledgments—We thank Daniela Novick and Darren Baker for providing IFNAR1-EC and the DB2, AA3, 46.10, and 117.7 antibodies; Ester Feldmesser for help in the gene array analyses; and Prof. Yoram Shechter for help in the binding experiments.

REFERENCES

1. Haller, O., Kochs, G., and Weber, F. (2006) *Virology* **344,** 119–130
2. Platanias, L. C. (2005) *Nat. Rev. Immunol.* **5,** 375–386
3. Theofilopoulos, A. N., Baccala, R., Beutler, B., and Kono, D. H. (2005) *Annu. Rev. Immunol.* **23,** 307–336
4. Pestka, S., Krause, C. D., and Walter, M. R. (2004) *Immunol. Rev.* **202,** 8–32
5. Brierley, M. M., and Fish, E. N. (2002) *J. Interferon Cytokine Res.* **22,** 835–845
6. Stark, G. R., Kerr, I. M., Williams, B. R., Silverman, R. H., and Schreiber, R. D. (1998) *Annu. Rev. Biochem.* **67,** 227–264
7. Platanias, L. C., and Fish, E. N. (1999) *Exp. Hematol.* **27,** 1583–1592
8. Rosenblum, M. G., Yung, W. K., Kelleher, P. J., Ruzicka, F., Steck, P. A., and Borden, E. C. (1990) *J. Interferon Res.* **10,** 141–151
9. Grumbach, I. M., Fish, E. N., Uddin, S., Majchrzak, B., Colamonici, O. R., Figulla, H. R., Heim, A., and Platanias, L. C. (1999) *J. Interferon Cytokine Res.* **19,** 797–801
10. Rani, M. R., Foster, G. R., Leung, S., Leaman, D., Stark, G. R., and Ransohoff, R. M. (1996) *J. Biol. Chem.* **271,** 22878–22884
11. Jaks, E., Gavutis, M., Uze, G., Martal, J., and Piehler, J. (2007) *J. Mol. Biol.* **366,** 525–539
12. Cajean-Feroldi, C., Nosal, F., Nardeux, P. C., Gallet, X., Guymarho, J., Baychelier, F., Sempe, P., Tovey, M. G., Escary, J. L., and Eid, P. (2004) *Biochemistry* **43,** 12498–12512
13. Lutfalla, G., Holland, S. J., Cinato, E., Monneron, D., Reboul, J., Rogers, N. C., Smith, J. M., Stark, G. R., Gardiner, K., Mogensen, K. F., Kerr, I. M., and Uze, G. (1995) *EMBO J.* **14,** 5100–5108
14. Kalie, E., Jaitin, D. A., Abramovich, R., and Schreiber, G. (2007) *J. Biol. Chem.* **282,** 11602–11611
15. Roisman, L. C., Piehler, J., Trosset, J. Y., Scheraga, H. A., and Schreiber, G. (2001) *Proc. Natl. Acad. Sci. U. S. A.* **98,** 13231–13236
16. Roisman, L. C., Jaitin, D. A., Baker, D. P., and Schreiber, G. (2005) *J. Mol. Biol.* **353,** 271–281
17. Chill, J. H., Quadt, S. R., Levy, R., Schreiber, G., and Anglister, J. (2003) *Structure* **11,** 791–802
18. Li, Z., Strunk, J. J., Lamken, P., Piehler, J., and Walz, T. (2008) *J. Mol. Biol.* **377,** 715–724
19. de Weerd, N. A., Samarajiwa, S. A., and Hertzog, P. J. (2007) *J. Biol. Chem.* **282,** 20053–20057
20. Uze, G., Schreiber, G., Piehler, J., and Pellegrini, S. (2007) *Curr. Top. Microbiol. Immunol.* **316,** 71–95
21. Sidhu, S. S., Lowman, H. B., Cunningham, B. C., and Wells, J. A. (2000) *Methods Enzymol.* **328,** 333–363
22. Piehler, J., and Schreiber, G. (1999) *J. Mol. Biol.* **289,** 57–67
23. Lamken, P., Lata, S., Gavutis, M., and Piehler, J. (2004) *J. Mol. Biol.* **341,** 303–318
24. Reichel, A., Schaible, D., Furoukh, N. A., Cohen, M., Schreiber, G., and Piehler, J. (2007) *Anal. Chem.* **79,** 8590–8600
25. Gavutis, M., Jaks, E., Lamken, P., and Piehler, J. (2006) *Biophys. J.* **90,** 3345–3355
26. Gavutis, M., Lata, S., Lamken, P., Muller, P., and Piehler, J. (2005) *Biophys. J.* **88,** 4289–4302
27. Strunk, J. J., Gregor, I., Becker, Y., Li, Z., Gavutis, M., Jaks, E., Lamken, P., Walz, T., Enderlein, J., and Piehler, J. (2008) *J. Mol. Biol.* **377,** 725–739
28. Lata, S., Gavutis, M., and Piehler, J. (2006) *J. Am. Chem. Soc.* **128,** 6–7
29. Jacobs, S., Hazum, E., Shechter, Y., and Cuatrecasas, P. (1979) *Proc. Natl. Acad. Sci. U. S. A* **76,** 4918–4921
30. Rubinstein, M., and Pestka, S. (1981) *Methods Enzymol.* **78,** 464–472
31. Jaitin, D. A., Roisman, L. C., Jaks, E., Gavutis, M., Piehler, J., Van der Heyden, J., Uze, G., and Schreiber, G. (2006) *Mol. Cell Biol.* **26,** 1888–1897
32. Jaitin, D. A., and Schreiber, G. (2007) *J. Interferon Cytokine Res.* **27,** 653–664
33. Smyth, G. K., and Speed, T. (2003) *Methods* **31,** 265–273
34. Smyth, G. K. (2004) *Stat. Appl. Genet. Mol. Biol.* **3,** Article 3
35. Reiner, A., Yekutieli, D., and Benjamini, Y. (2003) *Bioinformatics* **19,** 368–375
36. Piehler, J., Roisman, L. C., and Schreiber, G. (2000) *J. Biol. Chem.* **275,**

40425–40433
37. Marchetti, M., Monier, M. N., Fradagrada, A., Mitchell, K., Baychelier, F., Eid, P., Johannes, L., and Lamaze, C. (2006) *Mol. Biol. Cell* **17,** 2896–2909
38. Wagner, T. C., Velichko, S., Chesney, S. K., Biroc, S., Harde, D., Vogel, D., and Croze, E. (2004) *Int. J. Cancer* **111,** 32–42
39. Pearce, K. H., Jr., Cunningham, B. C., Fuh, G., Teeri, T., and Wells, J. A. (1999) *Biochemistry* **38,** 81–89
40. Marijanovic, Z., Ragimbeau, J., van der Heyden, J., Uze, G., and Pellegrini, S. (2007) *Biochem. J.* **407,** 141–151
41. Subramaniam, P. S., and Johnson, H. M. (2004) *FEBS Lett.* **578,** 207–210
42. Saleh, A. Z., Fang, A. T., Arch, A. E., Neupane, D., El Fiky, A., and Krolewski, J. J. (2004) *Oncogene* **23,** 7076–7086
43. Marijanovic, Z., Ragimbeau, J., Kumar, K. G., Fuchs, S. Y., and Pellegrini, S. (2006) *Biochem. J.* **397,** 31–38
44. Severa, M., Remoli, M. E., Giacomini, E., Ragimbeau, J., Lande, R., Uze, G., Pellegrini, S., and Coccia, E. M. (2006) *J. Leukocyte Biol.* **79,** 1286–1294
45. Claudinon, J., Monier, M. N., and Lamaze, C. (2007) *Biochimie* (*Paris*) **89,** 735–743
46. Damdinsuren, B., Nagano, H., Wada, H., Noda, T., Natsag, J., Marubashi, S., Miyamoto, A., Takeda, Y., Umeshita, K., Doki, Y., Dono, K., and Monden, M. (2007) *Hepatol. Res.* **37,** 77–83
47. Ito, K., Tanaka, H., Ito, T., Sultana, T. A., Kyo, T., Imanaka, F., Ohmoto, Y., and Kimura, A. (2004) *Eur. J. Haematol.* **73,** 191–205
48. Liu, J., Plotnikov, A., Banerjee, A., Suresh Kumar, K. G., Ragimbeau, J., Marijanovic, Z., Baker, D. P., Pellegrini, S., and Fuchs, S. Y. (2008) *Biochem. Biophys. Res. Commun.* **367,** 388–393
49. 49 Kumar, K. G., Varghese, B., Banerjee, A., Baker, D. P., Constantinescu, S. N., Pellegrini, S., and Fuchs, S. Y. (2008) *J. Biol. Chem.* **283,** 18566–18572
50. Gakovic, M., Ragimbeau, J., Francois, V., Constantinescu, S. N., and Pellegrini, S. (2008) *J. Biol. Chem.* **283,** 18522–18529
51. Ahmed, C. M., and Johnson, H. M. (2006) *J. Immunol.* **177,** 315–321